ION CHANNELS, RECEPTORS AND TRANSPORTERS

The role of TMEM16A (ANO1) and TMEM16F (ANO6) in cell migration

**K. S. Jacobsen · K. Zeeberg · D. R. P. Sauter ·
K. A. Poulsen · E. K. Hoffmann · A. Schwab**

Abstract Members of the TMEM16 family have recently been described as Ca^{2+}-activated Cl^- channels. They have been implicated in cancer and appear to be associated with poor patient prognosis. Here, we investigate the role of TMEM16 channels in cell migration, which is largely unknown. We focused on TMEM16A and TMEM16F channels that have the highest expression of TMEM16 channels in Ehrlich Lettre ascites (ELA) cells. Due to the lack of specific pharmacological modulators, we employed a miRNA approach and stably knocked down the expression of TMEM16A and TMEM16F channels, respectively. Migration analysis shows that TMEM16A KD clones are affected in their directional migration, whereas TMEM16F KD clones show a 40 % reduced rate of cell migration. Moreover, TMEM16A KD clones have a smaller projected cell area, and they are rounder than TMEM16F KD clones. The morphological changes are linearly correlated with the directionality of cells. TMEM16A and TMEM16F, thus, have an important function in cell migration—TMEM16A in directional migration, TMEM16F in determination of the speed of migration. We conclude that TMEM16A and TMEM16F channels have a distinct impact on the steering and motor mechanisms of migrating ELA cells.

K. S. Jacobsen · K. Zeeberg · D. R. P. Sauter · K. A. Poulsen ·
E. K. Hoffmann (✉)
Department of Biology, August Krogh Building,
Universitetsparken 13, 2100 Copenhagen Ø, Denmark
e-mail: ekhoffmann@bio.ku.dk

A. Schwab
Institut für Physiologie II, Westfälische Wilhelms-Universität
Münster, Münster, Germany

Present Address:
K. Zeeberg
Department of General and Environmental Physiology,
Via Amendola 165/A, 70126 Bari, Italy

Introduction

Cell migration is involved in important physiological and pathophysiological processes ranging from embryogenesis to tumor metastases. On a cellular level, it is a process that involves the precise temporal and spatial integration of many components of the cellular migration machinery. One of these components, whose crucial role was appreciated only in recent years, is comprised of ion transport proteins. Numerous ion channels and transporters have been shown to be required for efficient migration of many different cell types (see [31, 32, 36] for review). Several general mechanisms have been identified, by which ion transport proteins impact on cell migration. They include but are not limited to the regulation of the cell volume and of the intracellular Ca^{2+} concentration ($[Ca^{2+}]_i$).

Many of the ion transport proteins that are part of the cellular migration machinery are involved in the regulation of the cell volume [15]. Based on this observation, we proposed a model that comprises local swelling at the cell front during the protrusion of the lamellipodium and local cell shrinkage at the rear part of the cell during its retraction [30]. By and large, this model was confirmed experimentally by showing (local) volume changes of migrating cells of up to ~30 % [12, 27, 38] and by revealing the functional expression of the respective transport proteins such as $K_{Ca}3.1$ channels, NHE1, NKCC1, or AQP1 either at the cell front or at the rear part of migrating cells [11, 18, 25, 33]. In order to induce local shrinkage, $K_{Ca}3.1$ channels need to cooperate with anion channels. In glioblastoma cells, ClC3 channels were proposed to constitute the major route for the required anion efflux [5, 21]. Since ClC3 indirectly acquires Ca^{2+} sensitivity via its interaction with Ca^{2+}/calmodulin-

dependent protein kinase II, its activity can be coordinated with that of K_{Ca} channels and other Ca^{2+} dependent cytoskeletal mechanisms of cell migration. Alternatively, volume-regulated anion channels were proposed to cooperate with $K_{Ca}3.1$ channels [26]. Cell migration is a Ca^{2+}-dependent process, and loading cells with the Ca^{2+} chelator BAPTA inhibits migration [7]. Thus, it is also likely that Ca^{2+}-activated Cl^- channels could be involved.

Recently, TMEM16A and B also called anoctamin 1 and 2 (or ANO 1 and 2) were identified as molecular correlates of Ca^{2+} sensitive Cl^- channels [4, 6, 29, 40]. TMEM16F or ANO6 was also recently shown to be a Ca^{2+}-activated Cl^- channel with delayed Ca^{2+} activation [10, 35]. To date, ten members of the TMEM16 gene family have been identified in mammals (TMEM16A-K (I is omitted) or ANO1–10). They are conserved throughout the eukaryotic kingdom and contain eight-pass transmembrane segments with the N and C termini located in the cytosol and a reentrant loop situated between TM5 and TM6 possibly comprising the pore domain [9, 13, 14]. Each member is predicted to have multiple isoforms being simultaneously expressed in a given cell [6]. Nonetheless, the TMEM16 family shows tissue-specific expression. mRNA abundance of all members has been assayed in murine tissue, showing that TMEM16A, F, G, H, J, and K (ANO1, -6, -7, -8, -9, and -10) are expressed in various epithelial tissues, while TMEM16B, C, D, and E (ANO2, -3, -4, and -5) are primarily expressed in neuronal and musculoskeletal tissues [28]. One study has shown that members of the TMEM16 family (especially TMEM16A, F, and K) often are expressed in the same tissue [19]. This observation could indicate that the family members work in concert compensating for each other upon disarrangements.

In the context of the present paper, it is noteworthy that TMEM16/ANO proteins have been known for some time to be upregulated in cancer and to be associated with poor patient prognosis [17]. Moreover, some studies pointed towards a role of TMEM16A/ANO1 channels in tumor cell migration [2, 24]. In the present study, we tested whether other TMEM16 isoforms also contribute to migration of Ehrlich Lettre ascites (ELA) cells, and whether they can compensate each other.

Materials and methods

Cell culture and generation of mTMEM16A and mTMEM16F stable knock-down Ehrlich Lettre ascites cell lines

Experiments were performed using ELA cells. Cells were kept at 37 °C with 5 % CO_2:95 % air and cultured in RPMI1640, with 10 % fetal bovine serum and 1 % penicillin/streptomycin added to the media. Cells were transfected with miR-16A-KD plasmid or miR-16F-KD (see construction of microRNA plasmids) plasmid using Lipofectamine 2000 (Invitrogen, Taastrup, Denmark) and incubated for 4 h, then resuspended in selection medium containing blasticidin (10 μg/ml). After 1 week of selection, single cells were picked and transferred to 96-well trays and allowed to grow into a full clone in the presence of blasticidin. Clones were screened for knockdown using qPCR and Western blot analysis. The selected clones were named TMEM16A-5, TMEM16A-7, TMEM16A-9, TMEM16F-10, TMEM16F-15, TMEM16F-16, and TMEM16K.

Construction of microRNA plasmids

Interfering microRNA (miRNA) KD of mTMEM16A and mTMEM16F was generated using BLOCK-iT™ Pol II miR RNAi expression vector kits (Invitrogen, Taastrup, Denmark). miRNA targeting mouse TMEM16A and TMEM16F were designed using the Invitrogen® online design tool generating sense and antisense single stranded DNA strings (ssDNA). DNA sequences were; TMEM16A-5 and 7: sense 5'-tgctggtaacttgcccattcctcatagttttggccac tgactgactatgaggagggcaagttac-3', TMEM16A-5 and 7: antisense 5 -cctggtaacttgccctcctcatagtcagtcagtggccaaaactatga ggaatgggcaagttacc-3', TMEM16A-9: sense 5'-tgctgtttg gaggaagccgagtagtcgtttggccactgactgacgactactccttcctccaaa-3', TMEM16A-9: antisense 5'-cctgtttggaggaaggagtagtcgtca gtcagtggccaaaacgactactcggcttcctccaaac-3', TMEM16F: sense 5'-tgctgtttagcgggagtttgatgtgcgttttggccactgactgacg cacatcactcccgctaaa-3', TMEM16F: antisense: 5'-cctgtttag cgggagtgatgtgcgtcagtcagtggccaaaacgcacatcaaactcccgctaaac-3', TMEM16K: sense 5'-tgctgagcatcagggctaagttcagggtttt ggccactgactgaccctgaactgccctgatgct-3', and TMEM16K: antisense 5'-cctgagcatcagggcagttcagggtcagtcagtggccaaaaccct gaacttagccctgatgctc-3'.

The two ssDNAs were annealed generating a dsDNA, which were then ligated into pcDNA™6.2-GW/EmGFP-miR generating miR-16A-KD, miR-16 F-KD, and miR-16 K-KD. Plasmids were transformed into OmniMax T1 *Escherichia coli* (Invitrogen, Taastrup, Denmark) and selected using spectinomycin as antibiotic (50 μg/μl). Plasmid inserts were confirmed by DNA sequencing.

Isolation of RNA, cDNA, and qPCR

Total RNA was isolated from ELA cells using NucleoSpin RNA II columns according to the manufacturer's protocol. cDNA was prepared in a total volume of 20 μl by hybridization of 500 ng oligo dT primers to 2 μg RNA at 65 °C for 5 min followed by extension at 42 °C for 50 min in the presence of 200 U Superscript II reverse transcriptase (Invitrogen, Brondby, Denmark), 500 μM dNTP, 10 μM DTT, 50 mM Tris–HCl, 75 mM KCl, and 3 mM $MgCl_2$, pH 8.3. Finally, the reverse transcription (RT) was

inactivated at 70 °C for 15 min. Real-time qPCR was performed in duplicates using a Stratagene MX4000 real-time PCR system and SYBR Green PCR master mix (ABI) in a total volume of 20 μl containing 1 μl of the RT reaction, 200 nM of primers, and 10 μl 2× MasterMix. Primers used for qPCR were: TMEM16 A 16A_for; 5'-gacctgggctatg aggttca-3', 16A_rev; 5'-ggctgatgtctttggggata-3'; TMEM16F 16F_for; 5'-gcagcccttggatcttatca-3', 16F_rev; 5'-tgctgtagctc aacggtgtc-3'; 16K_for; 5'tctgagtggaccagccttct-3', 16K_rev; agaagagtgaggcgaagcaa-3'; mouse β₂ microtubulin mB2m_for; 5'-attttcagtggctgctactcg-3', mB2m_rev; 5'-attttttccgttcttcagc-3', acidic ribosomal protein ARP_for; 5'-cgacctggaagtcca actac-3', ARP-rev; 5'-atctgcatctgcttg-3'. TMEM16 expression levels were normalized to the reference gene levels (mB2m and ARP), and the relative expression ratios were calculated using the equation:

$$E_{ratio} = \frac{E_{target}{}^{\Delta C(t)_{target}(control \div treated)}}{E_{ref}{}^{\Delta C(t)_{ref}(control \div treated)}}$$

Where E_{target} and E_{ref} are the amplification efficiencies for the target gene and the average of the two reference genes ARP and mB2m, respectively. $\Delta C(t)_{target}$ and $\Delta C(t)_{ref}$ are the change in $C(t)$ values for target and reference genes.

Gel electrophoresis and Western blotting

Cells were lysed in 95 °C lysis buffer (150 mM NaCl, 20 mM HEPES, 1 mM EDTA, 10 % Glycerol, 0.5 % Triton X-100, and 0.5 % SDS) with protease inhibitors (Roche Applied Science) and phosphatase inhibitors added. The lysates were subsequently homogenized, and the supernatant was collected by centrifugation. Protein concentrations were determined using Bio-Rad DC protein assay, and identical amounts of protein was added to each lane. SDS-polyacrylamide gel electrophoresis was performed using a 10 % gel (Invitrogen), and size-fractionated proteins were transferred to nitrocellulose membranes. The membranes were stained with Ponceau Red (Sigma) as a second control of identical protein loading in each lane and washed in TBST (10 mM Tris HCl, pH 7.5, 120 mM NaCl, and 0.1 % Tween 20) before being blocked in a 5 % nonfat dry milk and TBST solution. Membranes were incubated with primary antibody at following concentrations: TMEM16A; ab53212 (abcam) 1:50, TMEM16A; Ano1 AB (DOG1AB) 1:500; TMEM16F; sc-136932 contingent (Santa Cruz) 1:250, β-actin; A1978 (Sigma) 1:1,000. Membranes were washed in TBST before incubation with the secondary antibody (Sigma) 1:5,000. The protein bands were visualized using 5-bromo-4-chloro-3-indolyl phosphate-nitro blue tetrazolium (Kirkegaard and Perry Lab) and scanned.

Electrophysiology

Cells were grown on poly-L-lysin-coated coverslips. Whole-cell patch-clamp recordings were performed using the Axopatch 200B amplifier interfaced to a Digidata 1440A controlled by pClamp10 software (Molecular Devices). Analog signals were acquired at 2.5 kHz and filtered at 1 kHz. Patch electrodes were pulled from borosilicate glass and had an input resistance of 2.5–6 MΩ. All recordings were performed at room temperature (20 °C). The standard bath solution contained (in millimolar): 150 NaCl, 1.5 CaCl2, 1 MgCl2, 10 Glucose, 10 HEPES, pH 7.4, and osmolality 315 mOsm. The 1 μM free Ca^{2+} pipet solution contained (in millimolar): 100 CsAsp, 40 CsCl, 4.34 CaCl₂, 4 Na₂ATP, 1 MgCl₂, 5 EGTA, 10 HEPES, pH 7.2, and osmolality 295 mOsm.

Cell migration

Migration of ELA wild-type (wt) and ELA KD cells was assessed with a wound-healing assay. When the cell monolayers were confluent, a scratch was made with a fine pipette (width ~260 μm). Then, the culture medium was replaced with serum-free medium, and the cells were allowed to recover in the incubator for 1 h. The tissue culture flasks were thereafter sealed and placed in a heating chamber (37 °C) on the stage of an inverted microscope (Axiovert 25 or Axiovert 40C; ×10 or ×20; Zeiss, Oberkochen, Germany). Migration was monitored with a video camera for 4 h (Hamamatsu, Herrsching, Germany) and controlled by HiPic software (Hamamatsu). Images were analyzed in 15-min intervals by marking the outlines of individual cells semiautomatically at each time step with Amira software (TGS Inc., San Diego, CA, USA). These segmentation data were used for further processing. Migration was quantified as the movement of the cell center (geometric mean of the pixel positions within the cell outlines) and the rate determined as the displacement of the cell center with time (micrometer per minute). Translocation (micrometer) is the distance between the position of cells at the beginning and at the end of the experiment. The trajectories of individual cells were normalized to a common starting point ($t=0$ h). The cell area (square micrometers) is the appropriately scaled sum of all pixels inside the cell contours in two dimensions. The structural index ($SI=4\pi A/p^2$) reflects the "roundness" of a cell with A representing the cell area and p the cell perimeter. It is one for a circle and approaches zero for a very elongated cell. The directionality of cell migration during wound closure was assessed by calculating the velocity of migration perpendicular to the wound (micrometer per minute). The directionality index is the ratio of translocation and total path length. We analyzed at least $n=30$ cells from $\geq N=3$ experiments for each condition.
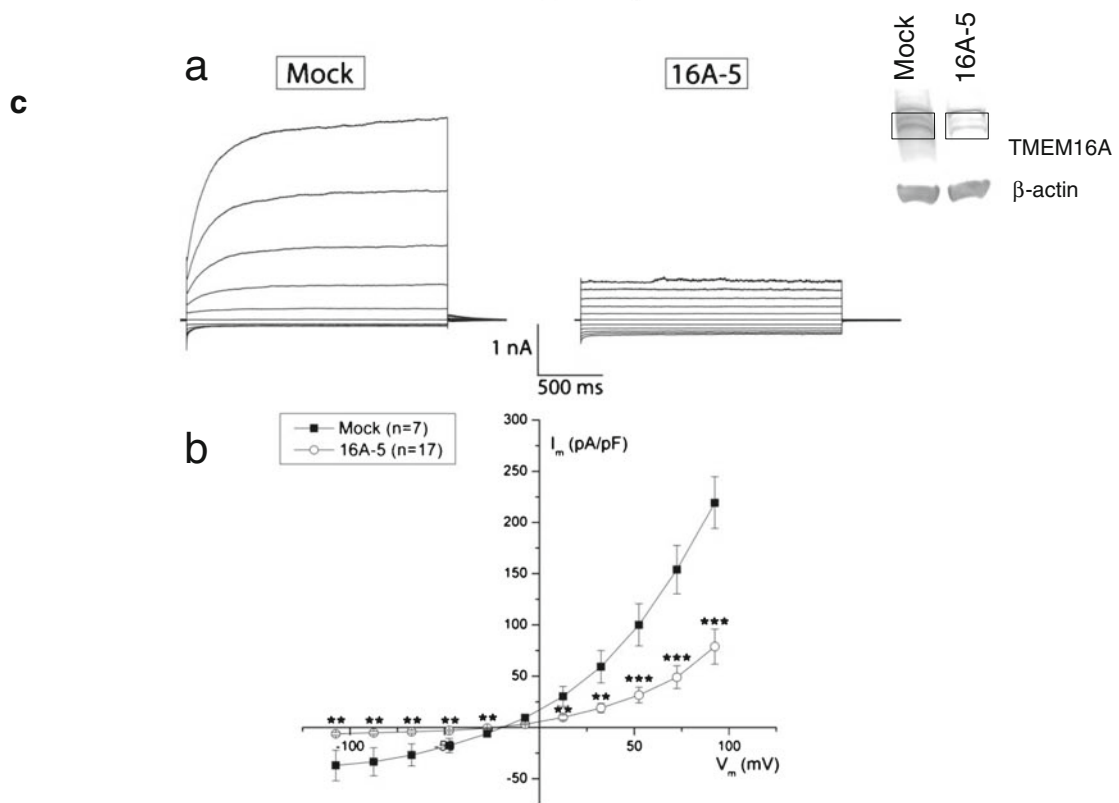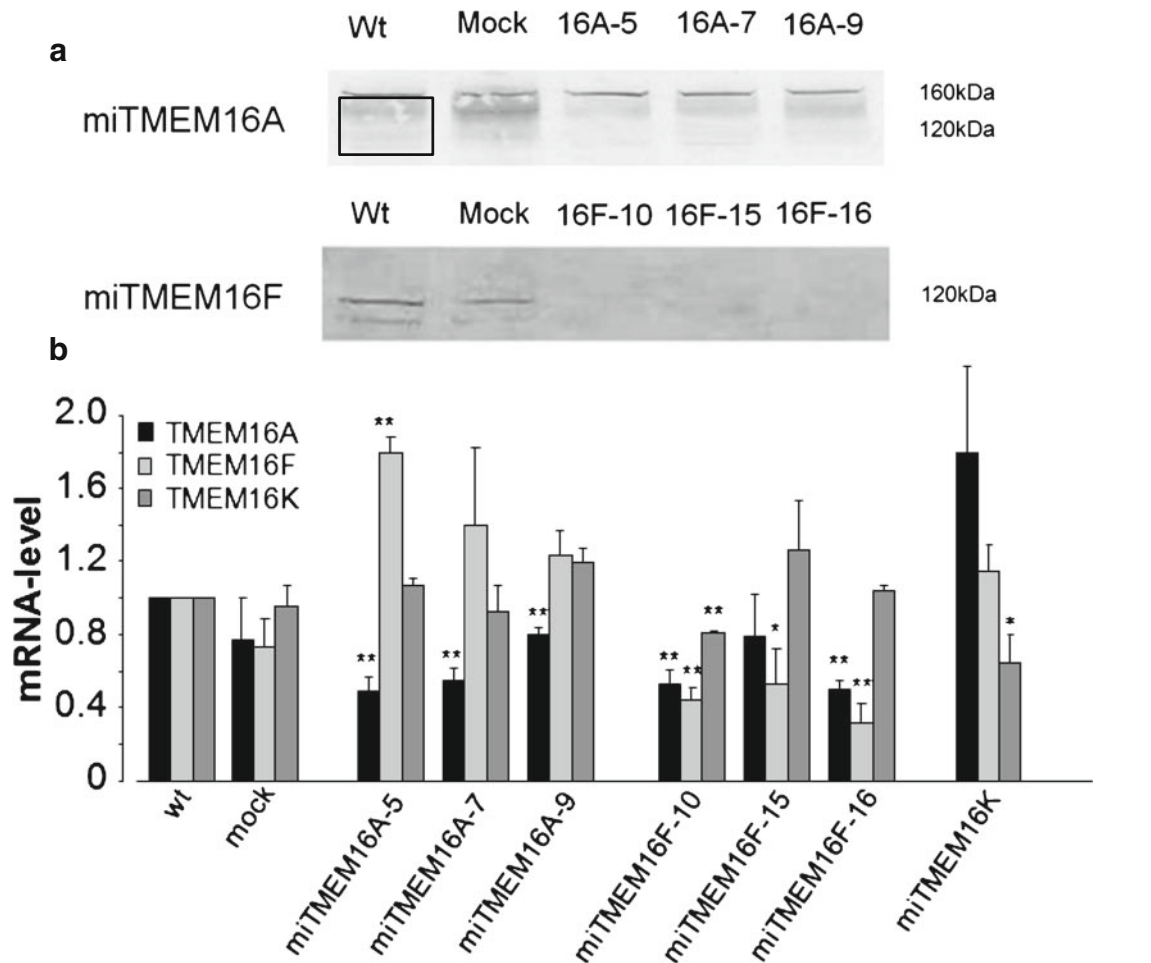
a

	Wt	Mock	16A-5	16A-7	16A-9	

miTMEM16A
160kDa
120kDa

	Wt	Mock	16F-10	16F-15	16F-16	

miTMEM16F
120kDa

b

c

a   Mock   16A-5

1 nA

500 ms

b

Mock (n=7)
16A-5 (n=17)

I_m (pA/pF)

V_m (mV)

◀ **Fig. 1** Verification of knock down of TMEM16A and F on protein and mRNA level. **a** SDS–polyacrylamide gel electrophoresis (10 % gel) of the three TMEM16A and the three TMEM16F knockdown clones compared to wild-type and mock clones. The membranes were stained with Ponceau Red (Sigma) as a control of identical protein loading in each lane. Membranes were incubated with primary antibody against TMEM16A; ab53212 (abcam) or TMEM16F; sc-136932 (Santa Cruz). TMEM16A is seen as a smear from 160–120 kDa (area inside the *box*). TMEM16A-5 and TMEM16A-7 show a clear downregulation of TMEM16A when compared to wt and mock, and in TMEM16A-9, a clear tendency towards downregulation is apparent. TMEM16F is seen as a band at 120 kDa and as a smaller isoform at 55 kDa. We were not able to quantify the protein bands because of the poor antibodies towards both TMEM16A and TMEM16F. The blot for TMEM16A is typical for $N=5$, and the blot for TMEM16F is typical for $N=3$. Five blots against TMEM16F were discarded because of too much unspecific binding. **b** Quantitative RT-PCR analysis of TMEM16A (*black*), F (*light gray*), and K (*dark gray*) relative mRNA levels in control, mock, three TMEM16A KD clones (TMEM16A-5,-7, and -9), three TMEM16F KD clones (TMEM16F-10, -15, and -16), and one TMEM16K KD clone. While a knockdown of TMEM16A led to an upregulation of TMEM16F, a knockdown of TMEM16F was accompanied by a downregulation of TMEM16A. Data are shown as means ± SEM, $N \geq 3$, $^*P<0.05$, and $^{**}P<0.01$. mRNA levels were normalized to the housekeeping genes acidic ribosomal protein and mouse β_2 microtubulin. **c** Whole-cell membrane currents (Im) from ELA cells stably transfected with TMEM16A-miRNA and mock vector as indicated. **a** Each panel shows currents elicited at different membrane potentials in the range of −100 to +100 mV in steps of 20 mV in the presence of 1 µM free intracellular Ca^{2+}. **b** Membrane currents measured at the end of voltage pulses (V_m) are plotted against the applied membrane potential after correction for the liquid-junction potential. The currents measured in miTMEM16A cells were significantly smaller than those of mock-transfected cells (**$P<0.01$ and ***$P<0.001$)

Statistics

All data are presented as representative original experiments or as means ± standard error of the mean (SEM). The statistical significance of differences was assessed with paired or unpaired Student's *t* test as appropriate. miTMEM16 clones were compared with the mock transfected clone. The level of significance was set to $p<0.05$.

Results

Verification of TMEM16A and TMEM16F knockdown in Ehrlich Lettre ascites cells

To investigate the role of the chloride channels TMEM16A and TMEM16F in cell migration, we generated stable TMEM16A and TMEM16F miRNA knockdown ELA cell lines. The KD cell lines were selected for constitutive expression of miRNA hairpins targeting mouse TMEM16A and TMEM16F. Twenty KD clones of each were screened for reduced TMEM expression and three of each (TMEM16A-5, -7 and -9 and TMEM16F-10, -15, and -16) were selected for further verification using Western blotting,

qPCR, and whole cell patch clamp. Figure 1a shows the efficiency of TMEM16A and TMEM16F knockdown at the protein level. Because of poor antibodies against both TMEM16A and TMEM16F, we were not able to quantify the bands. In all gels, however, miTMEM16A-5 and miTMEM16A-7 show a clear knockdown of TMEM16A, and in miTMEM16A-9, there is a tendency towards downregulation, too. In Fig 1c an extra blot showing the knockdown of TMEM16 A5 has been added, this time, including β-actin as a loading control. For TMEM16F, all three clones seem to be downregulated.

Using qPCR, we analyzed the mRNA expression levels of TMEM16A, 16 F, and 16 K in all cell lines (Fig. 1b). All miTMEM16A clones had a reduced TMEM16A mRNA expression level ranging between 50 (clone 5) and 80 % (clone 9) of the control level. However, the TMEM16F mRNA level was elevated to 180 % of the control level in miTMEM16A-5 clone. Similarly, there was a trend towards elevated TMEM16F expression in miTMEM16A-7 and -9 clones. TMEM16K expression level was not affected by the knockdown of TMEM16A (Fig. 1b). All selected miTMEM16F clones showed a reduced TMEM16F mRNA level. Notably, two of the three clones (miTMEM16F-10 and -16) also had reduced TMEM16A mRNA levels, ranging between 50 and 80 % of the respective control values. Clone miTMEM16F-10, furthermore, showed a reduced TMEM16K level as well (Fig. 1b). Whole cell patch clamp recordings of TMEM16A-5 showed a significant knockdown in current further supporting a successful knockdown of TMEM16A (Fig. 1c). This was not possible to do for TMEM16F, as the TMEM16A current was too dominating in ELA cells.

The role of TMEM16A and TMEM16F in cell migration

To investigate the role of TMEM16A and 16 F in cell migration, a scratch assay was used. The results of these experiments are depicted in Fig. 2. Figure 2a–c shows the trajectories of individual cells from the different clones normalized to common starting points. The statistical evaluation is presented in Fig. 2d. wt ELA cells migrated at a speed of 0.48±0.03 µm/min (Table 1) and covered 83.0±5.8 µm during the course of experiment (Fig. 2a and d). The transfection process itself does not alter the migratory behavior, since speed and translocation of mock-transfected cells are indistinguishable of those from wt cells (0.53±0.03 µm/min and 88.9±4.5 µm, respectively; Table 1, Fig. 2a and d). The migrational speed of the two miTMEM16A clones with higher KD efficiency (clones 5 and 7) was elevated by ~20 %, while that of clone 9, whose knockdown was less pronounced, was reduced by 17 % (Table 1). Nonetheless, the translocation was not affected in the two former miTMEM16A clones, while it was reduced in the latter one
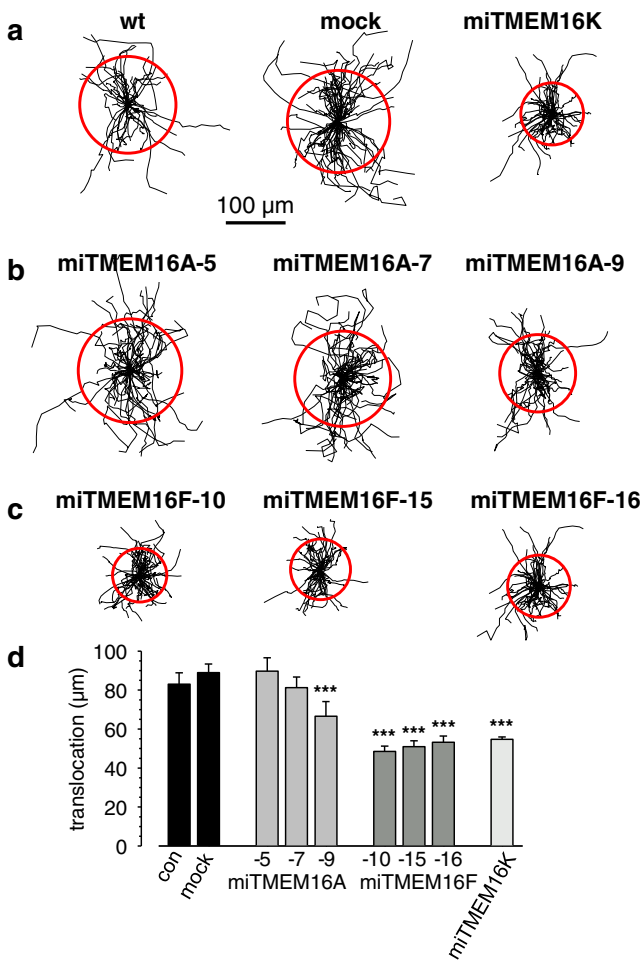
Fig. 2 Cell migration analysis. Trajectories of individual ELA wt cells, mock, and miTMEM16K cell clones (**a**), miTMEM16A clones (**b**), and miTMEM16F clones (**c**) monitored during a 4-h time period. All trajectories were normalized to a common starting point, which corresponds to the center of the circle. **d** Summation of average translocation which is given by the *circles* in Fig. 2a–c. Data are a representative of four or more independent experiments ± SEM with $n \geq 40$, *** indicates $P < 0.001$

Table 1 Analysis of cell migration in TMEM16A, 16F, and 16K KD clones

| | Wt | Mock | miTMEM16A | | | miTMEM16F | | | miTMEM16K |
			-5	-7	-9	-10	-15	-16	
Translocation (μm)	83.0±5.8	88.9±4.5	89.7±6.9	81.2±5.4	66.6±4.8**	48.5±2.7***	51.0±3.0***	53.2±3.2***	54.7±1.2***
Migratory speed (μm/min)	0.48±0.03	0.53±0.03	0.61±0.03	0.65±0.03**	0.44±0.02**	0.30±0.01***	0.29±0.01***	0.32±0.01***	0.29±0.02***
Directional migration (μm)	66.7±5.2	72.1±4.2	72.4±6.7	64.4±5.8	54.3±4.5***	36.4±2.6***	40.3±3.1***	34.8±3.3***	43.5±3.2***
Directionality index	0.72±0.03	0.69±0.02	0.59±0.03*	0.53±0.03*	0.62±0.03*	0.68±0.03	0.71±0.02	0.68±0.02	0.76±0.02*

The asterisks denote statistically differences between mock and KD clones

*$P<0.05$; **$P<0.01$; ***$P<0.001$, respectively

by ~25 % (Fig. 2b and d, Table 1). The behavior of the miTMEM16F clones was more homogeneous. Migration speed and translocation of all miTMEM16F KD clones were reduced on average by ~40 % (Fig. 2c and d, Table 1).

We next analyzed whether expression of TMEM16A and TMEM16F channels affect the directionality of ELA cell migration. In Fig. 3d and e, we plotted the movement of the cells into the wound as a function of time (movement into the "y-direction" as depicted in Fig. 3a). Interestingly, the faster miTMEM16A clones 5 and 7 did not advance further into the wound than wt and mock-transfected cells. Similarly, the delay of cells from the miTMEM16A-9 clone is larger than the reduction of the speed. Both observations point towards a defect in the directionality of migration of miTMEM16A cells. To confirm this idea, we calculated a directionality index, which represents the ratio of the
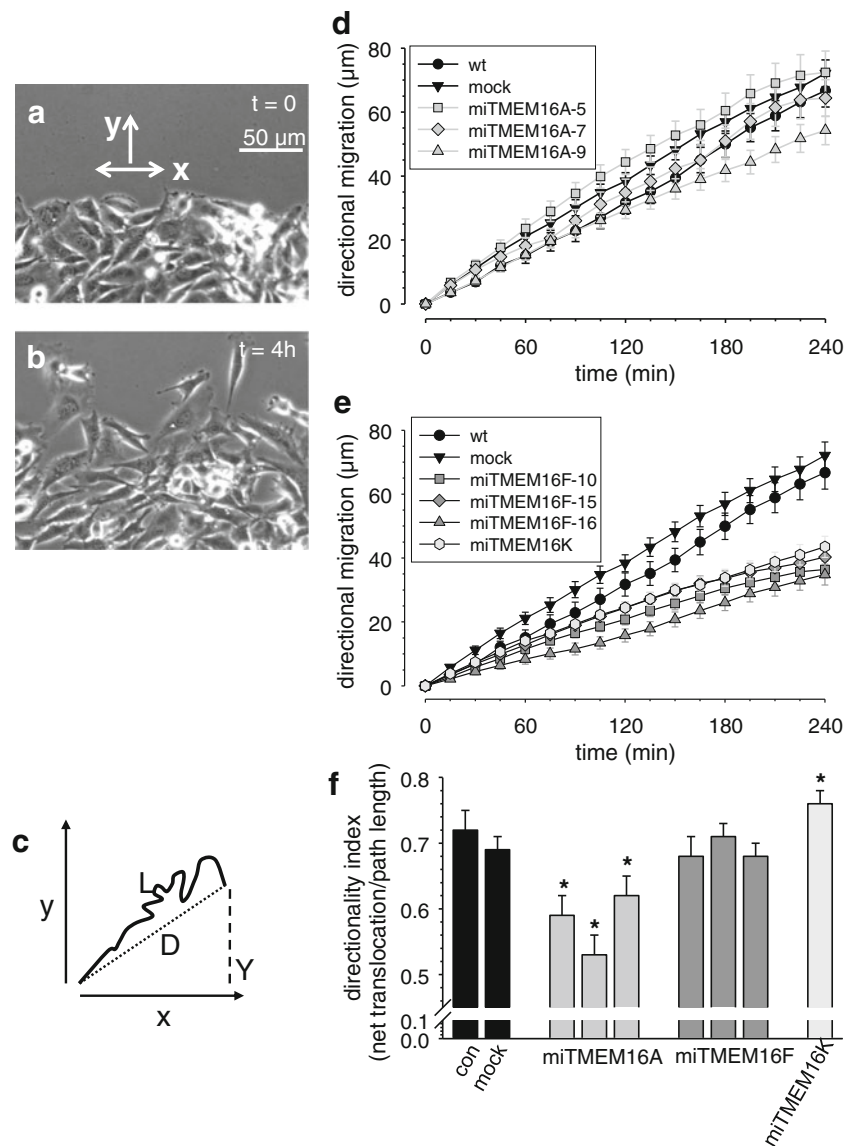
Fig. 3 Knockdown of TMEM16 channels affects directionality differentially. **a** and **b** Micrographs of the wound healing assay at the beginning of the experiment and at $t=4$ h. Migration into the wounded area is reflected by movement into the "y-direction" of a coordinate system. **c** Schematic representation of the analysis of directional migration. The directionality index is calculated as the ratio of net translocation **D** and total path length *L*. **d** and **e** Directional movement into the wound plotted as a function of time. **f** Comparison of the directionality indices of the different ELA cell clones. TMEM16A knockdown leads to an impaired directionality. Data is a representative of four or more independent experiments ± SEM with $n \geq 40$ cells. *Asterisk* indicates $P < 0.05$

distance traveled into the wound and the total distance covered during the course of the experiment (see Fig. 3c). Calculating the directionality index reveals that the directionality of miTMEM16A cells is impaired (Fig. 3f, Table 1). It is significantly smaller in all miTMEM16A cells than in wt or mock-transfected cells. Such a defect in directionality is not present in miTMEM16F cells. In these cells, migrational speed and directional migration into the wound are reduced proportionately (Fig. 3e and f, Table 1).

In Fig. 4, we compared the migratory phenotype of our different cell clones with the respective ratios of the mRNA

expression of TMEM16A and TMEM16F. Migratory speed (Fig. 4a) and directionality (Fig. 4b) are linearly correlated with the ratio of TMEM16A to TMEM16F mRNA. Thus, it seems that TMEM16A has a dampening effect on the migratory motor, while it supports directionality, and thereby persistent migration into a given direction. In contrast, TMEM16F has a positive effect on the migratory motor without affecting directionality. To lend further support to this interpretation, we also compared TMEM16A and TMEM16F mRNA levels in a miTMEM16K cell clone. We chose this cell clone, since the KD of TMEM16K was
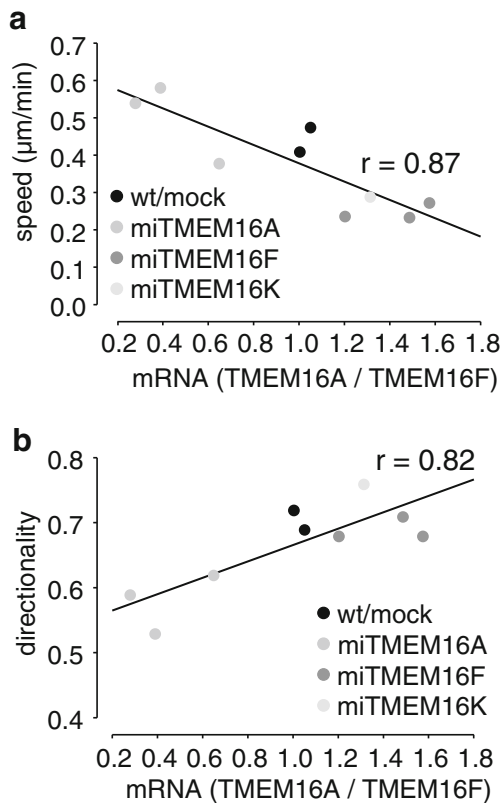
Fig. 4 mRNA ratio of TMEM16A and TMEM16F correlates with migratory behavior of ELA cell clones. **a** TMEM16A<TMEM16F mRNA correlates with increased migratory speed. **b** In contrast, directionality is higher when TMEM16A>TMEM16F mRNA

not very successful (−25 % on mRNA level) but, instead, it exhibited pronounced changes in TMEM16A (+80 %) and TMEM16F (+20 %) mRNA levels. Migratory behavior of miTMEM16K cells and their ratio of TMEM16A and F mRNA nicely fit to the linear correlation mentioned above. While the speed and translocation of the miTMEM16K cells are reduced, their directionality is increased (Figs. 2 and 3e, f).

TMEM16A and TMEM16F impact on cell morphology

Cl⁻ efflux in neutrophils was reported to result in cell spreading of neutrophil granulocytes [22, 23]. We therefore evaluated whether knockdown of TMEM16A or TMEM16F altered the spreading behavior of ELA cells and determined the projected cell area and the structural index. TMEM16A and TMEM16F knockdown affect the morphology of ELA cells differentially. miTMEM16A cells have a smaller projected cell area (Fig. 5a), and they are rounder (increased structural index; Fig. 5c) than miTMEM16F cells, which is consistent with a role of TMEM16A channels in cell spreading. The morphological changes are closely linked to the altered migratory behavior, since cell area and structural index are

linearly correlated with the directionality of cells (Fig. 5b and d). This also applies to the miTMEM16K cell clone. Finally, we tested whether morphological changes could be accounted for by an altered adhesive behavior. Cells were allowed to adhere for 45 min before adherent cells were counted. Neither TMEM16A nor TMEM16F knockdown changed cell adhesion (data not shown).

Discussion

In the present study, we performed a detailed analysis of the contribution of different TMEM16 channel isoforms to migration of the mouse mammary ELA cell line. We focused on TMEM16A and TMEM16F channels that have the highest expression of TMEM16 channels in ELA cells. Due to the lack of specific pharmacological modulators, we employed a miRNA approach and stably knocked down the expression of TMEM16A and TMEM16F channels, respectively. The key result of our study is that TMEM16A and TMEM16F channels are both required for optimal cell migration. However, they appear to affect different components of the cellular migration machinery, so that their knockdown elicits different migratory phenotypes. TMEM16A channels are involved in the steering process, while TMEM16F channels are part of the migratory "engine". Accordingly, knockdown of the two channels leads to impaired directionality and reduced translocation, respectively. The important question remains, by which mechanisms TMEM16A and TMEM16F elicit their differential effect on cell migration.

TMEM16A channels were shown to form Ca^{2+}-activated Cl^- channels [4, 6, 29, 40] that can be activated by cell swelling [1]. They can thereby act in concert with Ca^{2+} sensitive K^+ channels (e.g., $K_{Ca}3.1$) in mediating localized cell shrinkage at the rear part of migrating cells [19, 32]. Since $K_{Ca}3.1$ channels were shown to be involved in directional migration [34], it is conceivable that TMEM16A knockdown impairs directionality too. In addition, TMEM16A channels could also modify the intracellular Ca^{2+} concentration by regulating the cell membrane potential. When TMEM16A channels are activated by a rise of the intracellular Ca^{2+} concentration, the resulting Cl^- efflux will attenuate the hyperpolarization induced by the parallel activation of $K_{Ca}3.1$ channels. This would dampen Ca^{2+} influx by reducing the electrochemical driving force for Ca^{2+} ions. Along these lines, TMEM16A channels would affect the intracellular Ca^{2+} concentration in a similar way as TRPM4 channels [20]. This implies that the intracellular Ca^{2+} concentration of miTMEM16A cells is higher than that of wt or mock-transfected cells. The small and roundish morphology of miTMEM16A cells could then at least in part be due to increased myosin contraction [3]. In addition, the round morphology of miTMEM16A cells can also be explained on
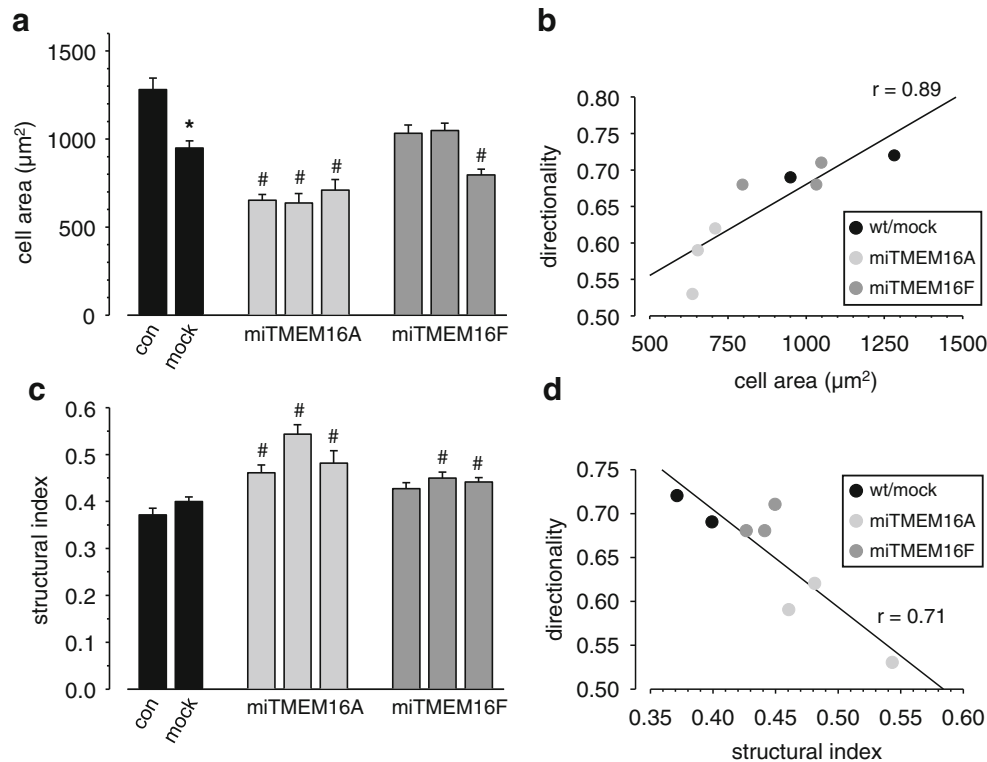
Fig. 5 Cell area and morphology. Cell area (**a**) and structural index (**c**) of wt, mock, miTMERM16A, and miTMEM16F cell clones were evaluated during migration experiments. miTMEM16A cells are smaller and more spherical than wt or mock-transfected cells. In contrast, the morphology of miTMEM16F cells hardly changed. Changes in cell area (**b**) and structural index (**d**) induced by TMEM16 knockdown are linearly correlated with directional motility. *Asterisk* denotes statistically significant difference between wt and mock clone ($P<0.05$), and *number sign* refers to differences between mock and miTMEM16 clones ($P<0.05$)

the basis of reduced Cl$^-$ efflux that is required for cell spreading [22].

TMEM16F channels are functionally quite distinct from TMEM16A channels. There is controversy about their biophysical properties. They are reported to constitute either a Ca^{2+}-activated anion channel [19, 35] or a Ca^{2+}-activated cation channel [39], and recently, Grubb et al. reported that $P_{Na}=0.334(\pm0.028)$ P_{Cl} in TMEM16F overexpressing HEK cells [10]. However, they also have nonconductive properties and mediate Ca^{2+}-dependent phospholipid scrambling [37, 39] and thereby regulate the phospholipid distribution in the plasma membrane. Normally, phosphatidylethanolamine or phosphatidylserine are predominantly found in the inner leaflet of the plasma membrane. The asymmetric phospholipid distribution can be abrogated by the activity of Ca^{2+}-dependent phospholipid scramblases [8, 37] or flippases [16]. In the context of the present study, it is important to note that migration involves the translocation of phosphatidylethanolamine within the plasma membrane, since inhibition of the scramblases or flippases impairs migration [8, 16]. Along these lines, the inhibition of migration of miTMEM16F cells could also be a consequence of impaired phospholipid translocation.

References

1. Almaca J, Tian Y, Aldehni F, Ousingsawat J, Kongsuphol P, Rock JR, Harfe BD, Schreiber R, Kunzelmann K (2009) TMEM16 proteins produce volume-regulated chloride currents that are reduced in mice lacking TMEM16A. J Biol Chem 284:28571–28578
2. Ayoub C, Wasylyk C, Li Y, Thomas E, Marisa L, Robe A, Roux M, Abecassis J, de Reynies A, Wasylyk B (2010) ANO1 amplification and

expression in HNSCC with a high propensity for future distant metastasis and its functions in HNSCC cell lines. Br J Cancer 103:715–726

3. Blaser H, Reichman-Fried M, Castanon I, Dumstrei K, Marlow FL, Kawakami K, Solnica-Krezel L, Heisenberg CP, Raz E (2006) Migration of zebrafish primordial germ cells: a role for myosin contraction and cytoplasmic flow. Dev Cell 11:613–627

4. Caputo A, Caci E, Ferrera L, Pedemonte N, Barsanti C, Sondo E, Pfeffer U, Ravazzolo R, Zegarra-Moran O, Galietta LJ (2008) TMEM16A: a membrane protein associated with calcium-dependent chloride channel activity. Science 322:590–594

5. Cuddapah VA, Sontheimer H (2010) Molecular interaction and functional regulation of ClC-3 by Ca^{2+}/calmodulin-dependent protein kinase II (CaMKII) in human malignant glioma. J Biol Chem 285:11188–11196

6. Duran C, Thompson CH, Xiao Q, Hartzell HC (2010) Chloride channels: often enigmatic and rarely predictable. Annu Rev Physiol 72:95–121

7. Espinosa-Tanguma R, O'Neil C, Chrones T, Pickering JG, Sims SM (2011) Essential role for calcium waves in migration of human vascular smooth muscle cells. Am J Physiol Heart Circ Physiol 301:H315–H323

8. Fan CW, Chen CY, Chen KT, Shen CR, Kuo YB, Chen YS, Chou YP, Wei WS, Chan EC (2012) Blockade of phospholipid scramblase 1 with its N-terminal domain antibody reduces tumorigenesis of colorectal carcinomas in vitro and in vivo. J Transl Med 10:254

9. Galietta LJ (2009) The TMEM16 protein family: a new class of chloride channels? Biophys J 97:3047–3053

10. Grubb S, Poulsen KA, Juul CA, Kyed T, Klausen TK, Larsen EH, Hoffmann EK (2013) TMEM16F (Anoctamin 6): an anion channel of delayed Ca^{2+} activation. J Gen Physiol. doi:10.1085/jgp.201210861

11. Haas BR, Sontheimer H (2010) Inhibition of the sodium–potassium–chloride cotransporter isoform-1 reduces glioma invasion. Cancer Res 70:5597–5606

12. Happel P, Moller K, Kunz R, Dietzel ID (2010) A boundary delimitation algorithm to approximate cell soma volumes of bipolar cells from topographical data obtained by scanning probe microscopy. BMC Bioinforma 11:323

13. Hartzell C, Putzier I, Arreola J (2005) Calcium-activated chloride channels. Annu Rev Physiol 67:719–758

14. Hartzell HC, Yu K, Xiao Q, Chien LT, Qu Z (2009) Anoctamin/TMEM16 family members are Ca^{2+}-activated Cl^- channels. J Physiol 587:2127–2139

15. Hoffmann EK, Lambert IH, Pedersen SF (2009) Physiology of cell volume regulation in vertebrates. Physiol Rev 89:193–277

16. Kato U, Inadome H, Yamamoto M, Emoto K, Kobayashi T, Umeda M (2013) Role for phospholipid flippase complex of ATP8A1 and CDC50A proteins in cell migration. J Biol Chem 288:4922–4934

17. Katoh M, Katoh M (2003) FLJ10261 gene, located within the CCND1-EMS1 locus on human chromosome 11q13, encodes the eight-transmembrane protein homologous to C12orf3, C11orf25, and FLJ34272 gene products. Int J Oncol 22:1375–1381

18. Klein M, Seeger P, Schuricht B, Alper SL, Schwab A (2000) Polarization of Na^+/H^+ and Cl^-/HCO_3^- exchangers in migrating renal epithelial cells. J Gen Physiol 115:599–608

19. Kunzelmann K, Tian Y, Martins JR, Faria D, Kongsuphol P, Ousingsawat J, Thevenod F, Roussa E, Rock J, Schreiber R (2011) Anoctamins. Pflugers Arch 462:195–208

20. Launay P, Fleig A, Perraud AL, Scharenberg AM, Penner R, Kinet JP (2002) TRPM4 is a Ca^{2+}-activated nonselective cation channel mediating cell membrane depolarization. Cell 109:397–407

21. McFerrin MB, Sontheimer H (2006) A role for ion channels in glioma cell invasion. Neuron Glia Biol 2:39–49

22. Menegazzi R, Busetto S, Dri P, Cramer R, Patriarca P (1996) Chloride ion efflux regulates adherence, spreading, and respiratory

burst of neutrophils stimulated by tumor necrosis factor-alpha (TNF) on biologic surfaces. J Cell Biol 135:511–522

23. Menegazzi R, Busetto S, Decleva E, Cramer R, Dri P, Patriarca P (1999) Triggering of chloride ion efflux from human neutrophils as a novel function of leukocyte beta 2 integrins: relationship with spreading and activation of the respiratory burst. J Immunol 162:423–434

24. Ruiz C, Martins JR, Rudin F, Schneider S, Dietsche T, Fischer CA, Tornillo L, Terracciano LM, Schreiber R, Bubendorf L, Kunzelmann K (2012) Enhanced expression of ANO1 in head and neck squamous cell carcinoma causes cell migration and correlates with poor prognosis. PLoS One 7:e43265

25. Saadoun S, Papadopoulos MC, Hara-Chikuma M, Verkman AS (2005) Impairment of angiogenesis and cell migration by targeted aquaporin-1 gene disruption. Nature 434:786–792

26. Schneider L, Klausen TK, Stock C, Mally S, Christensen ST, Pedersen SF, Hoffmann EK, Schwab A (2008) H-ras transformation sensitizes volume-activated anion channels and increases migratory activity of NIH3T3 fibroblasts. Pflugers Arch 455:1055–1062

27. Schneider SW, Pagel P, Rotsch C, Danker T, Oberleithner H, Radmacher M, Schwab A (2000) Volume dynamics in migrating epithelial cells measured with atomic force microscopy. Pflugers Arch 439:297–303

28. Schreiber R, Uliyakina I, Kongsuphol P, Warth R, Mirza M, Martins JR, Kunzelmann K (2010) Expression and function of epithelial anoctamins. J Biol Chem 285:7838–7845

29. Schroeder BC, Cheng T, Jan YN, Jan LY (2008) Expression cloning of TMEM16A as a calcium-activated chloride channel subunit. Cell 134:1019–1029

30. Schwab A, Wojnowski L, Gabriel K, Oberleithner H (1994) Oscillating activity of a Ca^{2+}-sensitive K^+ channel: a prerequisite for migration of transformed Madin–Darby canine kidney focus cells. J Clin Invest 93:1631–1636

31. Schwab A, Nechyporuk-Zloy V, Fabian A, Stock C (2007) Cells move when ions and water flow. Pflugers Arch 453:421–432

32. Schwab A, Fabian A, Hanley PJ, Stock C (2012) Role of ion channels and transporters in cell migration. Physiol Rev 92:1865–1913

33. Schwab A, Gabriel K, Finsterwalder F, Folprecht G, Greger R, Kramer A, Oberleithner H (1995) Polarized ion transport during migration of transformed Madin–Darby canine kidney cells. Pflugers Arch 430:802–807

34. Sciaccaluga M, Fioretti B, Catacuzzeno L, Pagani F, Bertollini C, Rosito M, Catalano M, D'Alessandro G, Santoro A, Cantore G, Ragozzino D, Castigli E, Franciolini F, Limatola C (2010) CXCL12-induced glioblastoma cell migration requires intermediate conductance $Ca2^+$-activated K^+ channel activity. Am J Physiol Cell Physiol 299:C175–C184

35. Shimizu T, Iehara T, Sato K, Fujii T, Sakai H, Okada Y (2013) TMEM16F is a component of a Ca^{2+}-activated Cl^- channel but not a volume-sensitive outwardly rectifying Cl^- channel. Am J Physiol Cell Physiol 304:C748–C759

36. Stock C, Schwab A (2009) Protons make tumor cells move like clockwork. Pflugers Arch 458:981–992

37. Suzuki J, Umeda M, Sims PJ, Nagata S (2010) Calcium-dependent phospholipid scrambling by TMEM16F. Nature 468:834–838

38. Watkins S, Sontheimer H (2011) Hydrodynamic cellular volume changes enable glioma cell invasion. J Neurosci 31:17250–17259

39. Yang H, Kim A, David T, Palmer D, Jin T, Tien J, Huang F, Cheng T, Coughlin SR, Jan YN, Jan LY (2012) TMEM16F forms a Ca^{2+}-activated cation channel required for lipid scrambling in platelets during blood coagulation. Cell 151:111–122

40. Yang YD, Cho H, Koo JY, Tak MH, Cho Y, Shim WS, Park SP, Lee J, Lee B, Kim BM, Raouf R, Shin YK, Oh U (2008) TMEM16A confers receptor-activated calcium-dependent chloride conductance. Nature 455:1210–1215